Escape trajectories of single-beam optically trapped micro-particles in a transverse fluid flow

Fabrice Merenda, Gerben Boer, Johann Rohner, Guy Delacrétaz and René-Paul Salathé

Advanced Photonics Laboratory
Ecole Polytechnique Fédérale de Lausanne, Station 17, CH-1015 Lausanne, Switzerland
fabrice.merenda@epfl.ch

Abstract: We have studied the transverse and axial equilibrium positions of dielectric micro-spheres trapped in a single-beam gradient optical trap and exposed to an increasing fluid flow transverse to the trapping beam axis. It is demonstrated that the axial equilibrium position of a trapped micro-sphere is a function of its transverse position in the trapping beam. Moreover, although the applied drag-force acts perpendicularly to the beam axis, reaching a certain distance r_0 from the beam axis ($r_0/a \simeq 0.6$, a being the sphere radius) the particle escapes the trap due to a breaking axial equilibrium before the actual maximum transverse trapping force is reached. The comparison between a theoretical model and the measurements shows that neglecting these axial equilibrium considerations leads to a theoretical overestimation in the maximal optical transverse trapping forces of up to 50%.

OCIS codes: (140.7010) Trapping, (170.4520) Optical confinement and manipulation, Microfluidic systems

References and links

1. D. G. Grier, "A revolution in optical manipulation," Nature **424**, 810–816 (2003).
2. M. Ozkan, M. Wang, C. Ozkan, R. Flynn, A. Birkbeck, and S. Esener, "Optical manipulation of objects and biological cells in microfluidic devices," Biomed. Microdevices **5**, 61–67 (2003).
3. J. Enger, M. Goksor, K. Ramser, P. Hagberg, and D. Hanstorp, "Optical tweezers applied to a microfluidic system," Lab. Chip **4**, 196–200 (2004).
4. J. Glückstad, "Microfluidics: Sorting particles with light," Nat. Mater. **3**, 9–10 (2004).
5. M. M. Wang, E. Tu, D. E. Raymond, J. M. Yang, H. C. Zhang, N. Hagen, B. Dees, E. M. Mercer, A. H. Forster, I. Kariv, P. J. Marchand, and W. F. Butler, "Microfluidic sorting of mammalian cells by optical force switching," Nat. Biotechnol. **23**, 83–87 (2005).
6. S. L. Neale, M. P. Macdonald, K. Dholakia, and T. F. Krauss, "All-optical control of microfluidic components using form birefringence," Nat. Mater. **4**, 530–533 (2005).
7. K. C. Neuman and S. M. Block, "Optical trapping," Rev. Sci. Instrum. **75**, 2787–2809 (2004).
8. A. Ashkin, J. M. Dziedzic, J. E. Bjorkholm, and S. Chu, "Observation of a Single-Beam Gradient Force Optical Trap for Dielectric Particles," Opt. Lett. **11**, 288–290 (1986).
9. G. Roosen, "La lévitation optique de sphères," Can. J. Phys. **57**, 1260–1279 (1979).
10. A. Ashkin, "Forces of a Single-Beam Gradient Laser Trap on a Dielectric Sphere in the Ray Optics Regime," Biophys. J. **61**, 569–582 (1992).
11. J. P. Barton, D. R. Alexander, and S. A. Schaub, "Theoretical determination of net radiation force and torque for a spherical particle illuminated by a focused laser beam," J. Appl. Phys. **66**, 4594–4602 (1989).
12. K. F. Ren, G. Greha, and G. Gouesbet, "Radiation Pressure Forces Exerted on a Particle Arbitrarily Located in a Gaussian-Beam by Using the Generalized Lorenz-Mie Theory, and Associated Resonance Effects," Opt. Commun. **108**, 343–354 (1994).

#10213 - $15.00 USD Received 4 January 2006; revised 3 February 2005; accepted 10 February 2006

13. W. H. Wright, G. J. Sonek, and M. W. Berns, "Parametric Study of the Forces on Microspheres Held by Optical Tweezers," Appl. Opt. **33**, 1735–1748 (1994).
14. A. Rohrbach and E. H. K. Stelzer, "Trapping forces, force constants, and potential depths for dielectric spheres in the presence of spherical aberrations," Appl. Opt. **41**, 2494–2507 (2002).
15. D. Ganic, X. S. Gan, and M. Gu, "Exact radiation trapping force calculation based on vectorial diffraction theory," Opt. Express **12**, 2670–2675 (2004).
16. O. Moine and B. Stout, "Optical force calculations in arbitrary beams by use of the vector addition theorem," J. Opt. Soc. Am. B **22**, 1620–1631 (2005).
17. S. Sato, M. Ishigure, and H. Inaba, "Optical Trapping and Rotational Manipulation of Microscopic Particles and Biological Cells Using Higher-Order Mode Nd-Yag Laser-Beams," Electron. Lett. **27**, 1831–1832 (1991).
18. A. Mazolli, P. A. M. Neto, and H. M. Nussenzveig, "Theory of trapping forces in optical tweezers," Proc. R. Soc. London Ser. A-Math. Phys. Eng. Sci. **459**, 3021–3041 (2003).
19. H. Felgner, O. Muller, and M. Schliwa, "Calibration of Light Forces in Optical Tweezers," Appl. Opt. **34**, 977–982 (1995).
20. N. B. Simpson, D. McGloin, K. Dholakia, L. Allen, and M. J. Padgett, "Optical tweezers with increased axial trapping efficiency," J. Mod. Opt. **45**, 1943–1949 (1998).
21. A. T. O'Neill and M. J. Padgett, "Axial and lateral trapping efficiency of Laguerre-Gaussian modes in inverted optical tweezers," Opt. Commun. **193**, 45–50 (2001).
22. N. Malagnino, G. Pesce, A. Sasso, and E. Arimondo, "Measurements of trapping efficiency and stiffness in optical tweezers," Opt. Commun. **214**, 15–24 (2002).
23. P. Torok, P. Varga, Z. Laczik, and G. R. Booker, "Electromagnetic Diffraction of Light Focused through a Planar Interface between Materials of Mismatched Refractive-Indexes - an Integral-Representation," J. Opt. Soc. Am. A **12**, 1605–1605 (1995).
24. P. Torok, P. Varga, Z. Laczik, and G. R. Booker, "Electromagnetic Diffraction of Light Focused through a Planar Interface between Materials of Mismatched Refractive-Indexes - an Integral-Representation -errata," J. Opt. Soc. Am. A **12**, 1605–1605 (1995).
25. S. Hell, G. Reiner, C. Cremer, and E. H. K. Stelzer, "Aberrations in Confocal Fluorescence Microscopy Induced by Mismatches in Refractive-Index," J. Microsc.-Oxford **169**, 391–405 (1993).
26. K. C. Neuman, E. A. Abbondanzieri, and S. M. Block, "Measurement of the effective focal shift in an optical trap," Opt. Lett. **30**, 1318–1320 (2005).
27. J. Happel and H. Brenner, eds., *Low Reynolds Number Hydrodynamics*, 2nd ed. (Kluwer Academic, Dordecht, the Netherlands, 1991).
28. H. C. van de Hulst, "Light Scattering by Small Particles," pp. 114–227 (Dover Press, New York, 1981).
29. P. C. Ke and M. Gu, "Characterization of trapping force in the presence of spherical aberration," J. Mod. Opt. **45**, 2159–2168 (1998)
30. E. Theofanidou, L. Wilson, W. J. Hossack and J. Arlt, "Spherical aberration correction for optical tweezers," Opt. Commun. **236**, 145 (2004).
31. Y. Roichman, A. Waldron, E. Gardel and D. G. Grier, "Performance of optical traps with geometric aberrations," Appl. Opt., in press (2005).

1. Introduction

The use of optical forces for trapping, manipulating and sorting particles or living cells in microfluidic devices is a growing field of research, with potential applications in biotechnology and gene technology [1, 2, 3, 4, 5, 6, 7]. The most widely applied technique for obtaining a 3D optical trap for micron-sized dielectric particles consists in coupling a collimated laser beam into a high numerical-aperture microscope objective. Provided that the numerical-aperture is sufficiently high, the force due to the field-gradient can overcome the forces due to back-scattered light, thus a three-dimensional optical trap is created. This optical trapping technique, first reported by Ashkin *et al.* [8], is commonly referred as optical tweezers or single-beam gradient optical trap.

When considering the combination of optical tweezers and microfluidic systems, the trapped dielectric particle has to sustain flows in a direction perpendicular to the beam axis, hence in these circumstances the most important characteristic of an optical tweezers is its maximal *transverse* trapping force. Actual theoretical predictions for the maximal transverse trapping forces of optical tweezers - that rely on ray-optics [9, 10] or on more rigorous calculations of the electro-magnetic fields and the Maxwell stress-tensor at the particle boundaries [11, 12,

#10213 - $15.00 USD Received 4 January 2006; revised 3 February 2005; accepted 10 February 2006

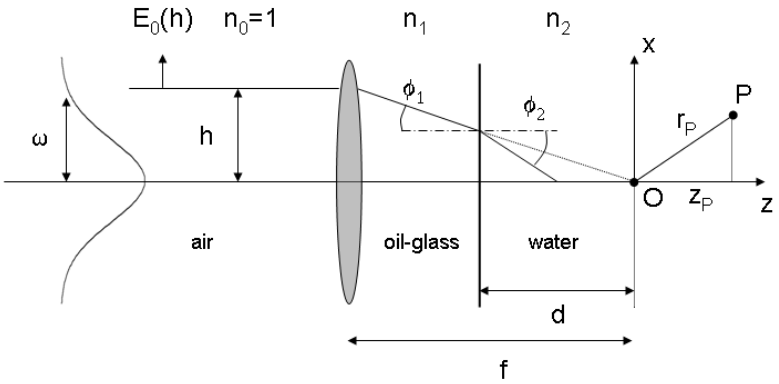

Fig. 1. Focusing light with a high-NA microscope objective, through a planar interface of mismatched index. The azimuth angle θ is not shown due to symmetry.

13, 14, 15, 16] - are commonly based on computing the radial force profile along the directions orthogonal to the beam axis. It is thus implicitly assumed that the particle only displaces radially (orthogonally to the beam axis) and stays in the focal plane of the focused laser beam. However, as this was already observed by Sato *et al.* [17] and Ashkin [10], and theoretically proposed by Mazolli *et al.* [18], this is not correct. When considering an optically trapped particle submitted to an increasing transverse liquid flow, as the drag-force increases the microsphere displaces from its resting equilibrium position - located somewhat above the focus - *both* in the radial and the axial directions, before it finally escapes the trap.

In this article we report an experimental study of the escape trajectories of optically trapped polystyrene microspheres exposed to an increasing transverse liquid flow by means of the standard drag-force technique [13, 19, 20, 21, 22]. A mathematical model which can predict optical forces both for on-axis and off-axis positions of the microsphere was also used. The escape trajectories deduced with this model are compared to the experimental measurements. It is shown that, reaching a certain distance from the optical axis, the particle escapes the trap due to a breaking *axial* equilibrium, before the actual maximum transverse force is reached, and that this has to be taken into account for a reliable mathematical prediction of the maximal transverse trapping forces.

2. Theory

The hybrid mathematical model we used combines the rigorous vectorial electromagnetic-field model for the high numerical-aperture (NA) laser beam focusing proposed by Török *et al.* [23, 24] - taking into account spherical aberrations due to the coverglass-water refractive index mismatch - and the simple ray-optics reflection-refraction model at the sphere boundary developed by Roosen [9].

2.1. EM-field calculations

As described in Fig. 1, we consider a collimated Gaussian beam focused by an oil-immersion high-NA microscope objective (MO) obeying the Abbe sine condition $h = f sin\phi_1$, where f is the focal length in oil (of refractive index n_1). The origin O of the system of coordinates is positioned at the focus, as if the beam were focused into the index-matching oil. The position vector $\mathbf{r}_P$, pointing from O to P, is given in spherical coordinates by

$$\mathbf{r}_P = [x_P, y_P, z_P] = r_P[sin\phi_P cos\theta_P, sin\phi_P sin\theta_P, cos\phi_P] \quad (1)$$

#10213 - $15.00 USD Received 4 January 2006; revised 3 February 2005; accepted 10 February 2006

No refractive index change between the immersion oil and the coverglass is considered. The interface between the coverglass and the water containing the dielectric particles to be trapped is located at $z = -d$. The angle of incidence at the interface is denoted by ϕ_1 and the angle of refraction by ϕ_2. The time-independent components of the electric field $\mathbf{e} = (e_x, e_y, e_z)$ at any point P to the right of the interface (Fig. 1) are expressed as a linear combination of three integral terms $I_n^{(e)}$, $n = 0, 1, 2$

$$\begin{aligned} e_x &= -iK[I_0^{(e)} + I_2^{(e)} cos(2\theta_P)] \\ e_y &= -iKI_2^{(e)} sin(2\theta_P) \\ e_z &= -2KI_1^{(e)} cos(\theta_P) \end{aligned} \tag{2}$$

where

$$K = \frac{\pi n_1 f}{\lambda_0} \frac{e_0}{\sqrt{n_1}} \tag{3}$$

and

$$\begin{aligned} I_0^{(e)}(r_P, z_P) &= \int_0^\alpha exp(-\gamma^2 sin^2\phi_1)(cos\phi_1)^{1/2} sin\phi_1 exp[ik_0\psi(\phi_1, \phi_2, -d)] \\ &\quad \times (\tau_s + \tau_p cos\phi_2) J_0(k_1 r_P sin\phi_1) exp(ik_2 z_P cos\phi_2) d\phi_1 \\ I_1^{(e)}(r_P, z_P) &= \int_0^\alpha exp(-\gamma^2 sin^2\phi_1)(cos\phi_1)^{1/2} sin\phi_1 exp[ik_0\psi(\phi_1, \phi_2, -d)] \\ &\quad \times \tau_p sin\phi_2 \times J_1(k_1 r_P sin\phi_1) exp(ik_2 z_P cos\phi_2) d\phi_1 \\ I_2^{(e)}(r_P, z_P) &= \int_0^\alpha exp(-\gamma^2 sin^2\phi_1)(cos\phi_1)^{1/2} sin\phi_1 exp[ik_0\psi(\phi_1, \phi_2, -d)] \\ &\quad \times (\tau_s - \tau_p cos\phi_2) \times J_2(k_1 r_P sin\phi_1) exp(ik_2 z_P cos\phi_2) d\phi_1 \end{aligned} \tag{4}$$

The integral terms $I_n^{(e)}$ are modified from Török *et al.* [23] to accommodate for a Gaussian profile at the MO back-pupil, adding an extra term $exp(-\gamma^2 sin^2\phi_1)$ where $\gamma = f/\omega$, ω being the half Gaussian width of the incident collimated beam. α is the semi-aperture angle of the lens (in media n_1, $NA = n_1 sin\alpha$), τ_p and τ_s are the Fresnel transmission coefficients at the glass-water interface, and J_n are the Bessel functions of the first kind, order n. The wavenumbers read $k_0 = k_1/n_1 = k_2/n_2 = 2\pi/\lambda_0$ and the focal length $f = n_1 h_{max}/NA$, where h_{max} is the effective radius of the MO back-pupil. ψ is the aberration function defined by

$$\psi(\phi_1, \phi_2, -d) = -d(n_1 cos\phi_1 - n_2 cos\phi_2) \tag{5}$$

Finally the constant e_0 in (3) is the peak amplitude of the electric field incident onto the MO back-pupil, which is in contact with air ($n_0 = 1$). Similar expressions as (2-4) exist for the magnetic-field vectors [23]. In the following, the time-averaged Poynting vector

$$\mathbf{I} = <\mathbf{S}> = \frac{1}{2}\mathscr{R}\{\mathbf{e} \times \mathbf{h}^*\} \tag{6}$$

will be used to describe the local light intensity I, which is necessary for the computation of the optical force on dielectric particles (next section 2.2).

It is well known that focusing light through a planar interface of mismatched refractive indexes creates a focus shift relative to its position in a uniform medium [25, 26], in addition to extending the axial point spread function of the lens. For small focusing depths the position of the focus (defined as the position of highest intensity) in media n_2 shifts fairly linearly with the position of the interface

$$z_{focus} = -k_f d \tag{7}$$

#10213 - $15.00 USD Received 4 January 2006; revised 3 February 2005; accepted 10 February 2006

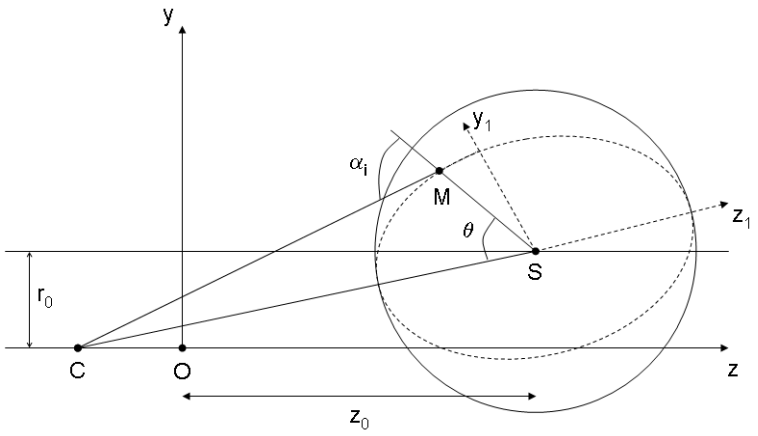

Fig. 2. Geometry for the calculation of the momentum transfer between the beam and the dielectric sphere. The forces are calculated using a ray-optics approximation in the plane of incidence defined by (y_1, z_1), and then projected onto the (y,z) axes.

where k_f is the linearity constant for this focus shift. In the paraxial limit $k_f = 1 - n_2/n_1$, but for high-NA systems a more precise estimation is to be done numerically.

For the sake of comparison, we will also use the ray-optics approach for the beam focusing, which approximates the light intensity I by

$$I = I_0 exp\{-2\gamma^2 sin^2\phi_2\} f^2 cos\phi_2 \frac{1}{r_P^2}; \tag{8}$$

in the same spherical coordinates. Note that in this case it is assumed that $\gamma = \frac{f}{\omega}$ with f being defined by $f = n_2 h_{max}/NA$ neglecting thus the effect of the mismatched coverglass-water interface.

2.2. Optical Force on a dielectric sphere

The force exerted by the focused laser beam on a dielectric sphere is calculated using a ray-optics approximation. In order to obtain optical forces for both on-axis and off-axis sphere positions, the momentum transfer corresponding to a pencil of light impinging on particular surface element dA of the sphere is first obtained in a system of coordinates attached to the plane of incidence, and then projected on the optical system of coordinates, following Roosen [9].

As shown in Fig. 2, let z be the optical axis and $S = (0, r_0, z_0)$ the center of the dielectric sphere of radius a. M is the impact point of a particular ray and C is the center of curvature corresponding to the wavefront impinging on the sphere surface at M. The plane of incidence is then defined by CSM, whose orthogonal system of coordinates is (x_1, y_1, z_1), and has its center in S (z_1 being the unity vector in the direction $\overline{CS}$, and y_1 lying in the plane of incidence and being orthogonal to z_1). In this second system of coordinates, a ray of intensity I impinging in M at an angle of incidence α_i on a surface element dA of the sphere induces an elementary force $d\mathbf{F}_1$

$$\begin{aligned} dF_{z_1} &= \frac{n_2 I}{c} cosi \Big[cos(\alpha_i - \theta) + Rcos(\alpha_i + \theta) \\ &\quad - T^2 \frac{cos(2\alpha_r - \alpha_i - \theta) + Rcos(\alpha_i + \theta)}{1 + R^2 + 2Rcos(2\alpha_r)} \Big] dA \end{aligned}$$

#10213 - $15.00 USD Received 4 January 2006; revised 3 February 2005; accepted 10 February 2006

$$dF_{y_1} = \frac{n_2 I}{c} cosi\Big[sin(\alpha_i-\theta)+Rsin(\alpha_i+\theta) - T^2\frac{sin(2\alpha_r-\alpha_i-\theta)+Rsin(\alpha_i+\theta)}{1+R^2+2Rcos(2\alpha_r)}\Big]dA \quad (9)$$

where n_2 is the index of refraction of the media surrounding the sphere, α_r is the angle of refraction of the ray entering the sphere, R and T are the intensity reflection and transmission coefficients, and c is the speed of light in vacuum. Polarization effects are neglected by averaging R and T over the two polarization states.

The optical forces F_z and F_y on the whole sphere are obtained by projecting the elementary forces dF_{z_1} and dF_{y_1} along the y and z axis and by integration over the sphere surface, but only rays characterized by $\alpha_i < \pi/2$ (thus entering the sphere) are to be considered. For symmetry reasons, and since polarization effects are neglected, there is no difference between a displacement along the x-axis and the y-axis. In the following sections the displacements of the sphere center from the focus position will simply be given by its transverse (radial) and axial positions r_0 and z_0.

The forces are calculated either by computing the intensity term I and the incident angles α_i in eq. (9) using the ray-optics (RO) beam focusing model described by eq. (8) or by combining (9) to the vectorial diffraction (VD) focusing model, the local light intensity I and incident angle α_i being in this case found using (6).

Finally, since we are interested by the position of the sphere with respect to the effective focus position, a coordinate translation $z_0 \rightarrow z_0 - k_f d$ is necessary when using the VD model, according to (7).

2.3. Special considerations for the drag-force technique

The drag-force technique consists in testing the optical force against a viscous drag force, created by moving the fluid surrounding the trapped particle. Since a motorized x-y stage is used the applied drag-force is purely transverse to the beam axis, whereas the gravitational force is parallel to the beam axis. Thus the motion equations in the transverse and axial directions may be written as

$$\begin{aligned} m\ddot{r_0} &= F_r(r_0,z_0)+\beta v_r \\ m\ddot{z_0} &= F_z(r_0,z_0)-(\rho-\rho_{fluid})Vg \end{aligned} \quad (10)$$

where r_0 and z_0 are the radial and axial coordinates of the sphere center with respect to the focus, and m,ρ,V are respectively the sphere mass, density and the immersed volume. v_r is the speed of the fluid surrounding the sphere, and β is the proportionality factor for the viscous drag according to Faxen's law [27], describing the laminar viscous drag for a spherical particle of radius a which is displacing parallel to a very close planar surface (the microscope coverglass)

$$\beta = \frac{6\pi a\eta}{1-\frac{9}{16}(\frac{a}{b})+\frac{1}{8}(\frac{a}{b})^3-\frac{45}{256}(\frac{a}{b})^4-\frac{1}{16}(\frac{a}{b})^5} \quad (11)$$

where a is the sphere radius, b is the distance between the sphere center and the planar surface (the trapping depth) and η is the viscosity of the fluid.

Assuming that the transverse velocity v_r of the fluid surrounding the sphere increases linearly with time (a_r being the constant acceleration) and provided that the acceleration terms $m\ddot{r}_0$, $m\ddot{z}_0$ and the gravitational force are small compared to the other terms in (10) the time-dependent equilibrium of the trapped particle is described by the solutions of

$$F_r(r_0(t),z_0(t)) = -\beta a_r(t-t_0), \quad t \geq t_0 \quad (12)$$

$$F_z(r_0,z_0) = 0 \quad (13)$$

#10213 - $15.00 USD Received 4 January 2006; revised 3 February 2005; accepted 10 February 2006

Given that the transverse flow velocity can be controlled as described in the righthand side of (12), this equation provides a way for measuring the transverse optical forces. On the other hand, equation (13) may be solved numerically to find the theoretical microsphere axial equilibrium position z_0^{eq} as a unique function of its transverse position r_0.

2.4. Trapping efficiency

The trapping efficiency Q is a non-dimensional form of the optical trapping force defined by

$$\mathbf{Q} = \frac{c}{n_2 P}\mathbf{F} \tag{14}$$

c being the speed of light in vacuum, n_2 the index of refraction of the media surrounding the particle and P the beam power at the focus [10]. **Q** measures the momentum transfer efficiency from the laser beam to the particle, and is of particular interest when desiring to characterize the trap performance per unit power.

From an experimental point of view, the maximum transverse trapping efficiency, as measured using the drag-force technique, is related to the maximum flow velocity v_r^{max} that the trap can withstand through

$$Q_r^{max} = \frac{c}{n_2 P}\beta v_r^{max} \tag{15}$$

This is the quantity that is usually reported in experimental studies of the maximal transverse trapping force based on the drag-force technique.

3. Experimental

3.1. Set-Up

In our set-up, depicted on Fig. 3, the trapping light source is a cw (monomode) pigtailed laser diode (Bookam UC9**) emitting at $974nm$ and having a maximal output power of $100mW$. The output beam is collimated to a Gaussian diameter of $3.2mm$, and coupled into a high-NA oil-immersion objective via the fluorescence port of an inverted microscope (Leica DMIL). The focusing high-NA lens is a Leica C-PLAN $100X/1.25$ oil-immersion microscope-objective (MO). Its effective back-pupil radius and transmission were determined using two identical confocused objectives.

Table 1. Experiment parameters

Parameter Description	Symbol	Value	Units
MO num. aperture	NA	1.25	
MO back-pupil radius	h_{max}	2.5	mm
MO power transm.	T_P	53.5	%
Power at the focus	P	29-40	mW
Vacuum Wavelength	λ_0	974	nm
Focal shift	k_f	0.22	
Inc. beam radius	ω	3.2	mm
Bead radius	a	$2.5-3.5$	μm
Bead refr. index	n	1.59	
Bead vol. mass	ρ	1050	Kg/m^3
Acceleration	a_r	60	μms^{-2}
Trapping depth	b	10	μm

#10213 - $15.00 USD Received 4 January 2006; revised 3 February 2005; accepted 10 February 2006

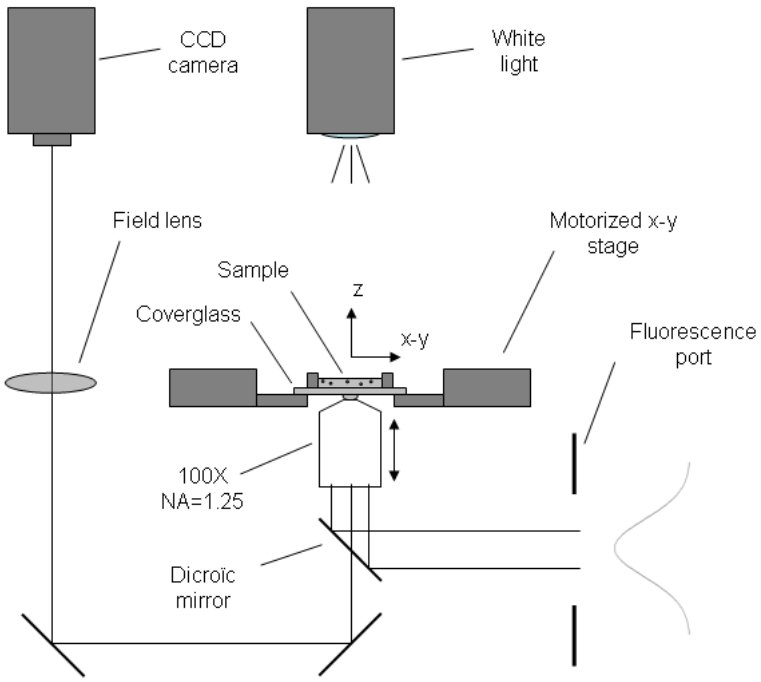

Fig. 3. Experimental set-up for optical trapping and video processing based measurement of the polystyrene bead positions, built around an inverted microscope.

The 5 and 7 μm diameter polystyrene micro-beads to be trapped (Dynospheres, Dyno Particles AS) are diluted in water and the sample-cell, whose bottom consists in a microscope coverglass, is mounted on a programmable x-y motorized stage (Märzhäuser) just above the MO. The beads are observed through the microscope dicroïc mirror (reflective for infrared and transparent for visible wavelengths) using a CCD camera connected to a video acquisition board. All relevant experimental parameters are listed in Tab.1.

3.2. 3D position measurement

The position of the trapped bead with respect to the focus is video-tracked with the microscope CCD camera. The axial position z_0 of the particle is determined from the analysis of the video sequences. Indeed, the microscope white-light illumination that is refracted (focused) by the bead produces an intensity spot on the CCD whose area A is related to the axial position z_0 of the bead with respect to the plane imaged on the CCD. This is illustrated in the two images of Fig. 4(a) which correspond to the extreme situations where no drag-force is applied (above), and where the drag-force is maximal and the bead is about to escape the trap (below). An experimental relationship $z_0 = z_0(A)$ was determined for both sphere sizes by observing a stuck microbead on the sample-cell bottom at different (defined) axial positions of the MO (graph in Fig. 4(b)), and fitted to a second order polynomial.

For this calibration, it must be taken into account that a given axial displacement of the MO does not correspond to an identical axial displacement of the focal plane in water, because of the coverglass-water refractive index mismatch [25, 26]. Indeed, an axial displacement Δz of the MO can be regarded as a shift of the coverglass-water interface in Fig. 1, thus the displacement

#10213 - $15.00 USD Received 4 January 2006; revised 3 February 2005; accepted 10 February 2006

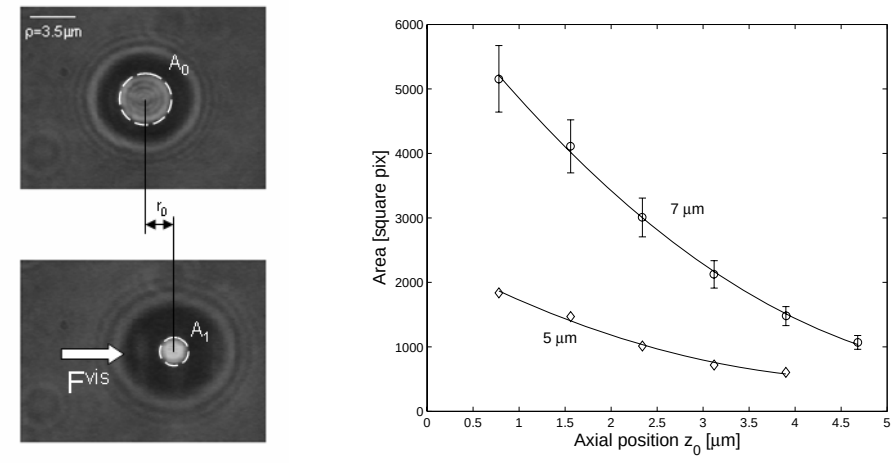

(a) (b)

Fig. 4. r-z position tracking by video-processing. (a) The trapped bead in its equilibrium position in still water (above) and when submitted to a transverse viscous force F^{vis} (below). The video processing computes the distance r_0 from the still position, and the axial position was experimentally related to the area of bright spot (A_0, A_1) resulting from the focusing of the white light apical illumination by the trapped bead. (b) Axial position calibration curves for both the 5 μm (diamonds $\diamond$) and the 7 μm beads (circles $\circ$), measured by observing a stuck microbead on the sample cell bottom and by stepwise displacing the MO axially.

$\Delta z'$ of the effective focus position in water is given by

$$\Delta z' = \Delta z - k_f \Delta z \quad \Rightarrow \quad \Delta z'/\Delta z = 1 - k_f \tag{16}$$

where k_f is the focus-shift parameter defined in (7). We calculated a ratio of $\Delta z'/\Delta z \simeq 0.78$ for our experimental parameters using the vectorial diffraction focusing model (according to the value of k_f given in Tab. 1).

With the bead-sizes we used (5 and 7 μm) the accuracy of the transverse position measurement with respect to the beam axis was estimated to be better than $0.1\mu m$. Concerning the axial position measurement, we were not able to ensure an accurate identical position of the laser focusing-plane and the plane imaged on the microscope CCD camera. The position of the laser focusing-plane depending on its precise collimation at the microscope objective back-pupil, and the plane imaged on the CCD relating to the accurate position of the CCD with respect to the focal plane of the microscope field-lens, the absolute axial position of the beads with respect to the laser focus could not be determined with an absolute precision greater than $1\mu m$. However, the *relative* precision of the axial position measurements is better than $0.3\mu m$.

3.3. Drag force experiment

The drag velocity v_r of a trapped bead was increased with a well-defined constant acceleration a_r with the help of the computer-controlled motorized $x-y$ stage, thus the instantaneous drag-force $-\beta a_r(t-t_0)$ applied to the particle was known at any time. From the recorded videos the $x-y$ positions and the area A of the bright spot could be recorded as a function of time. The experiment was repeated 5 times in each direction ($+x, -x, +y, -y$) using 5 and 7 μm beads,

#10213 - $15.00 USD Received 4 January 2006; revised 3 February 2005; accepted 10 February 2006

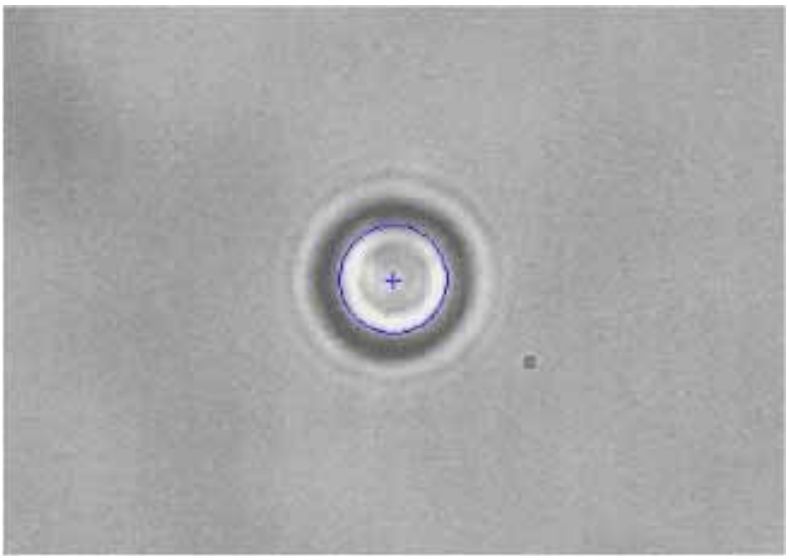

Fig. 5. (516 KB) - Movie of the drag-force experiment, showing the image analysis to retrieve the transverse and axial bead positions r_0 and z_0. The resting equilibrium position of the bead (no drag-force applied) is shown by the $+$ marker.

and the data for each direction was averaged. We decided for a trapping depth of $b \simeq 10\mu m$, which could be ensured with an accuracy of $\pm 2\mu m$.

Figure 5 shows a movie of the drag-force experiment. There is no drag-force at the beginning of the sequence. The transverse drag-force then increases linearly with time, until the bead escapes the trap. The images were taken at a video-rate of $10Hz$. At each time step the bead transverse and axial positions $r_0(t)$ and $z_0(t)$ are retrieved by image processing.

4. Results

4.1. Numerical results

The numerical solution of (13), predicting the axial equilibrium position z_0^{eq} of a trapped microsphere as a function of its transverse position r_0, is presented in Fig. 6(a) (solid line) for the parameters given in Tab. 1 and in the pure ray-optics (RO) approximation. Note that the r_0 and z_0 positions of the sphere with respect to the beam focus are normalized by the sphere radius a. The model predicts that, as the particle is displaced from the optical axis, its axial equilibrium position shifts in the positive (beam propagation) direction. The curve breaks at $r_0/a = 0.74$ because beyond this limit there exists no stable axial equilibrium position.

On the underlying graph of Fig. 6(b) the solid line shows the transverse force - in its normalized form $Q_r = cF_r/(n_2P)$ - calculated along the equilibrium trajectory $z_0^{eq}(r_0)$. It has to be emphasized that the the maximal transverse trapping efficiency, predicted to be $Q_r^{max} = 0.31$, is limited by the breaking of the axial trapping at that transverse position (escape positions and force are marked by stars $\star$).

Not considering the axial equilibrium aspects described above leads to a higher estimation of the maximal transverse force. Indeed, restricting the displacement of the particle to the focusing plane ($z_0 = 0$ for all r_0 as depicted by the dashed line in Fig. 6(a)) the resulting transverse force profile - shown by the dashed line of Fig. 6(b) - predicts a greater maximal transverse force corresponding to $Q_r^{max} = 0.41$. This maximal transverse force would be reached at a transverse

#10213 - $15.00 USD Received 4 January 2006; revised 3 February 2005; accepted 10 February 2006

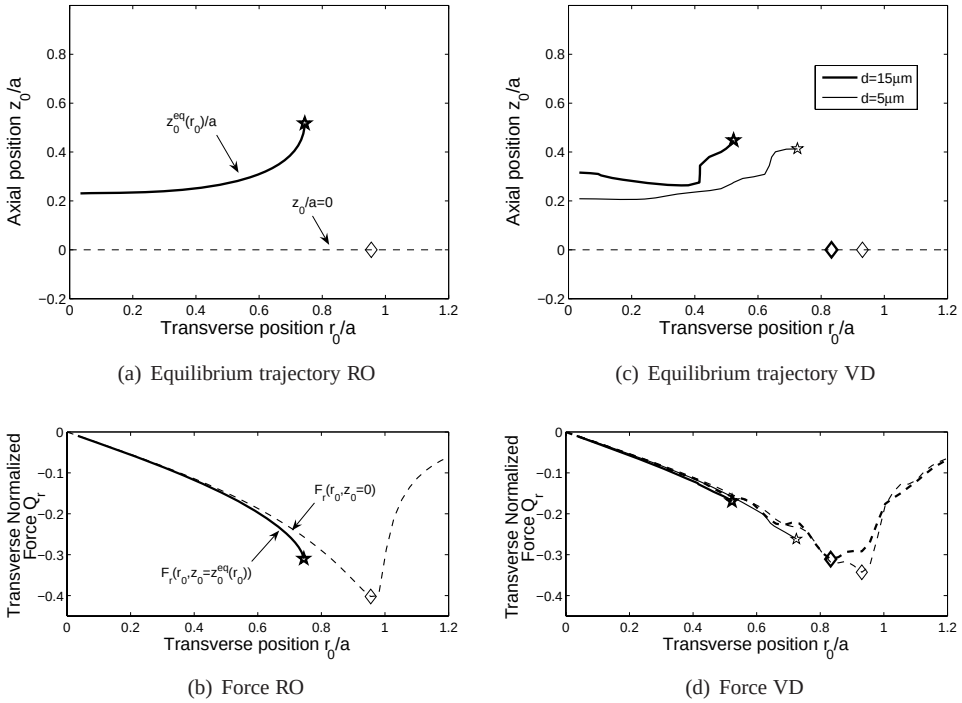

(a) Equilibrium trajectory RO

(c) Equilibrium trajectory VD

(b) Force RO

(d) Force VD

Fig. 6. Numerical results. (a) Pure ray-optics (RO) calculation of equilibrium trajectory $[r_0, z_0^{eq}(r_0)]$ (continuous line). The dashed line represents a pure transverse displacement in the focal plane. (b) Displacement-force curves in the RO approximation. Forces calculated along the equilibrium trajectory $[r_0, z_0^{eq}(r_0)]$ (continuous line) and along $[r_0, z_0 = 0]$ (dashed line) are compared. (c) Equilibrium trajectory according to the vectorial diffraction (VD) for the 7 μm beads at two different trapping depths ($5\mu m$ and $15\mu m$). (d) Displacement-force curves using the VD. Forces on the equilibrium trajectory (continuous lines) and in the focal plane (dashed lines) are compared.
The position axes are normalized by the sphere radius a and the force is given in the normalized form Q of (14). Note that the trajectory plots and the corresponding displacement-force plots have the same transverse axis scale. The stars ($\star$) and diamonds ($\diamond$) define the extreme transverse trapping positions and forces according to the two different approaches.

position of $r_0/a = 0.97$ (escape positions and force shown by diamonds $\diamond$).

Figure 6(c) presents the equilibrium trajectories as calculated using the vectorial diffraction (VD) model, for a $7\mu m$ diameter polystyrene bead at two different trapping depths ($d = 5\mu m$ and $d = 15\mu m$). Figure 6(d) shows the corresponding transverse forces calculated using the VD model. As for the RO model, the forces computed along $z_0 = 0$ (dashed lines) are compared to the transverse forces along the equilibrium trajectories $z_0^{eq}(r_0)$ (solid lines).

The VD model predicts that spherical aberrations (SA) strongly affect the equilibrium trajectory. At shallow trapping depths (very close to the coverglass), as the particle displaces away from the optical axis, the axial equilibrium position shifts monotonically in the positive direction. At a deeper trapping depth (bold solid line), the axial equilibrium position first shifts in the negative z-axis direction, then at larger r_0 it moves back in the positive z-direction.

SA are also predicted to further reduce the distance from the optical axis where the particle escapes, and subsequently the maximal transverse forces (Fig. 6(d)). Oppositely, the restoring

#10213 - $15.00 USD Received 4 January 2006; revised 3 February 2005; accepted 10 February 2006

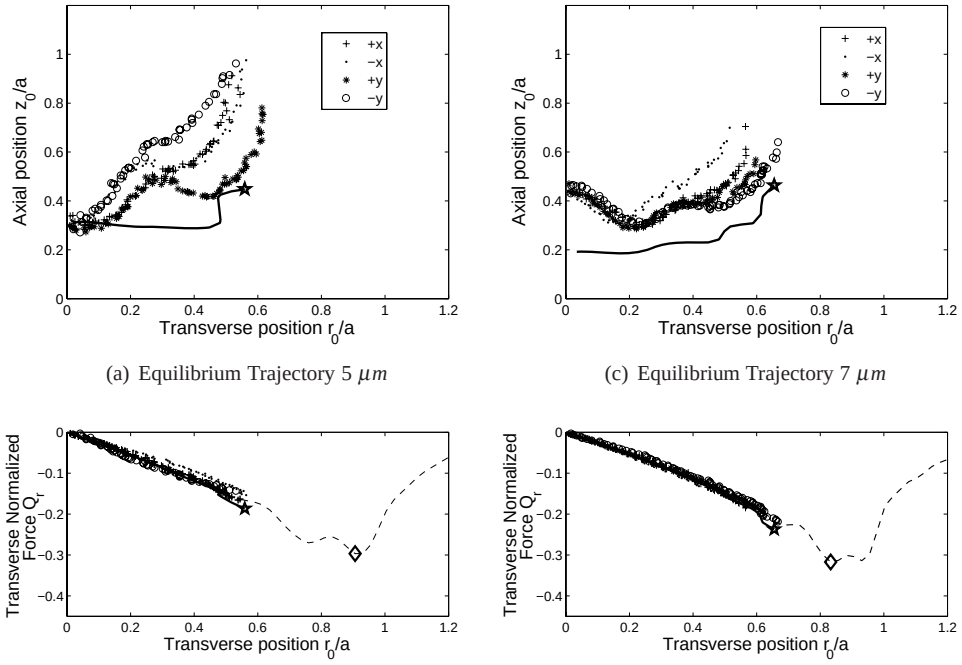

(a) Equilibrium Trajectory 5 μm

(c) Equilibrium Trajectory 7 μm

(b) Force 5 μm

(d) Force 7 μm

Fig. 7. Experimental results. **(a)** Measured trajectories in the 4 directions of the viscous drag, for the $5\mu m$ beads, compared to the theoretical trajectory (solid line). **(b)** Measured force-displacement curves corresponding to subfigure (a). Measurements are compared both to the theoretical force along the equilibrium trajectory (solid line - almost hidden by the measurements) and to the force calculated for a purely radial displacement (dashed line). **(c)** Same as (a), but for the $7\mu m$ beads. **(d)** Same as (b), but for the $7\mu m$ beads. Computed trajectories are for a trapping depth of $10\mu m$. The stars ($\star$) and diamonds ($\diamond$) define the extreme transverse trapping positions and forces according to the two different theoretical approaches.

force close to the optical axis (trap stiffness) is predicted to be only slightly affected by the SA.

The optical forces were calculated on a 36x30 grid ranging $r_0 = [0, 1.2a]$ and $z_0 = [0, a]$ to reduce the computation time. Intermediate values were linearly interpolated.

4.2. Experimental results

Figure 7(a) shows the observed escape trajectories of the $5\mu m$ beads. Escape trajectories have been investigated in the four drag-force directions $(+x, -x, +y, -y)$ in order to address the inhomogeneity of the trapping beam, and to ensure that the axial displacement is not related to a misalignment of the trapping beam with respect to the fluid flow. Note that each data point is an average of 5 drag-force measurements. As the particle is displaced away from the optical axis by the increasing drag-force, its axial equilibrium position z_0^{eq} shifts in the positive (beam propagation) direction. Small differences in the trajectory are put into evidence. The $+x$ and $-x$ plots are almost identical, while for the $+y$ and $-y$ plots a different axial displacement is observed, suggesting that these differences are due to slight optical misalignments.

The theoretical trajectory (solid line), computed using the VD model for a corresponding trapping depth of $10\mu m$, is compared to the measurements. Although the overall theoretical

#10213 - $15.00 USD Received 4 January 2006; revised 3 February 2005; accepted 10 February 2006

escape trajectory is not in fair agreement with the observed trajectories, the theoretical escape transverse position derived from this calculation is in agreement with the experimental mean value of $r_0/a = 0.56 \pm 0.5$ (standard deviation over the 20 drag-force experiments).

By contrast, the corresponding experimental transverse displacement-force curves in the four drag-directions (Fig. 7(b)) are in very good agreement with the computed data and the observed force plots corresponding to the four different drag-force directions are almost superposed. The measurements are compared to the force predictions by the VD model, either assuming that the particle follows the equilibrium trajectory $z_0^{eq}(r_0)$ (bold solid line, almost hidden by the measurements) or assuming that the particle displaces in the laser focusing plane $z_0 = 0$ (dashed line). In the first approach, the transverse escape position limits the theoretical maximal transverse force to a value of $Q_r^{max} \simeq 0.2$, in agreement with the experimental data. Using the second approach, generally adopted in the literature, the escape transverse position, corresponding to the absolute maximum of the restoring force, would be located at a distance close to $r_0/a = 0.9$, and the maximal transverse trapping force is overestimated.

The results obtained for the $7\mu m$ beads can be found in Fig. 7(c) (trajectories) and (d) (transverse displacement-force curves). The measured axial equilibrium position dependence on the transverse position is qualitatively different from that of the $5\mu m$ beads. A smaller absolute axial displacement is observed. Moreover, for small transverse displacements the axial equilibrium position first shifts in the negative direction, then at larger transverse positions moves back in the positive axial direction. The measured mean escape transverse position of $r_0/a = 0.59 \pm 0.6$ is correctly predicted by the VD model. The computed axial equilibrium position dependence on the transverse position reproduces the main observed characteristics, including an oscillating behaviour as the distance from the optical axis is increased. Nevertheless, an offset between the measurements and the theoretical curve remains.

As for the $5\mu m$ beads, the corresponding experimental transverse displacement-force curves (Fig. 7(d)) are in very good agreement with the computed data. The measurements are compared to the force predictions by the VD model, either assuming that the particle follows the equilibrium trajectory (bold solid line, almost hidden by the measurements) or assuming that the particle displaces in the laser focusing plane (dashed line). Taking into account the axial equilibrium failure, the observed maximal transverse force of $Q_r^{max} \simeq 0.2$ is correctly predicted. Neglecting the axial equilibrium failure the maximal transverse trapping force is significantly overestimated ($Q_r^{max} = 0.32$) as well as the escape distance from the optical axis ($r_0/a = 0.83$).

5. Discussion

There are two main observations to be retained. The first observation is that a trapped particle submitted to a purely transversal and increasing drag-force does not only displace transversally, as commonly supposed in the literature, but also axially. This behavior reflects the axial equilibrium position dependence on the transverse position in the trapping beam. To the best of our knowledge, this is the the first quantitative measurement for this particle axial equilibrium position dependence on the transverse position in the trapping beam. Both the experiments and the theoretical models show the same qualitative behavior, namely that the particle axial equilibrium position z_0^{eq} shifts in the positive direction as the particle is displaced away from the optical axis by the growing transverse drag-force.

The second important observation is that the stability of the particle in the trap relies on the simultaneous existence of a stable equilibrium in both the transverse and the axial directions. As a consequence, the escape of the particle results from the first equilibrium to be broken, in either one or the other direction. This has essential consequences on the maximal transverse force of the optical trap.

In the common approach for the theoretical prediction of the maximum transverse trapping

#10213 - $15.00 USD Received 4 January 2006; revised 3 February 2005; accepted 10 February 2006

forces, the transverse forces are computed along the directions orthogonal to the beam axis. The maximal transverse force then corresponds to the absolute maximum of the computed curve, taking place at transverse positions close to $r_0/a \simeq 0.8-0.9$. However, no *axial* equilibrium is theoretically possible at that distance from the optical axis. The appropriate way for predicting the transverse forces - only been followed by Mazolli et al. [18] - consists in calculating the transverse force along the equilibrium trajectory $z_0^{eq}(r_0)$. Consequently, the maximal transverse force corresponds to the transverse force at the furthermost transverse position where an axial equilibrium exists.

Our experimental measurements strongly sustain this theoretical approach because the measured escape transverse positions are not larger than $r_0/a \simeq 0.6$, in far better agreement with the transverse escape positions predicted by the broken axial equilibrium approach ($r_0/a \simeq 0.5-0.65$) than with the escape positions predicted by the absolute maximum transverse force within the laser focusing plane ($r_0/a \simeq 0.8-0.9$). Furthermore, the experimental maximal transverse trapping efficiencies of $Q_r^{max} \simeq 0.2$ are much closely predicted when simultaneously considering the transverse and axial equilibrium of the particle.

It must be emphasized that the present results are a particularity of the single-beam gradient optical trap and are due to the axial asymmetry of the force field. The gradient force field is symmetrical with respect of the laser focusing plane in the non-aberrated case, but the scattering force is not. Note that an optical trap based on two counter-propagating beams would not show this kind of behaviour, since the scattering forces are symmetrized.

Two models were used for the theoretical force calculations. The pure ray-optics approach (RO) was employed because it is the simplest and most widely applied model. This model already predicts the axial equilibrium position dependence on the transverse position in a qualitative manner, and also predicts that the particle escapes the trap due to a breaking of the axial equilibrium. However, its validity is limited to particle sizes far larger than the wavelength ($a >> \lambda$), it does not take into account spherical aberrations, and it is scale-invariant. For the 5 and $7\mu m$ we used, the escape distance and the maximal transverse trapping forces are overestimated, despite considering the axial trapping failure.

In order to take into consideration the particle size with respect to the beam focus size and the spherical aberration introduced by the coverslip-water interface, a hybrid theoretical model was used, combining the rigorous vectorial electromagnetic-field model for the high numerical-aperture laser beam focusing and the ray-optics approach for the force calculation (VD model). We computed the trajectories and forces for beads of 5 and 7 μm diameter.

When comparing the experimental trajectories z_0^{eq} to the trajectories predicted by the VD model a good agreement is observed in the displacement of the axial equilibrium position as a function of the transverse position for the $7\mu m$ beads. However, an offset of $\simeq 0.4\mu m$ is observed between the mathematical prediction and the measurement. This offset is related to the difficulties in determining the absolute position of the laser focusing plane with respect to the plane imaged on the CCD (see section 3.2). Note that this divergence corresponds to roughly $1/10$ of the sphere radius. The confidence in the relative axial displacements is much better.

The measured trajectories of the $5\mu m$ beads are not in good agreement with the theory, the measurements showing a greater axial displacement than predicted. It is to be expected that for smaller bead sizes the ray-optics approximation for the optical force computation we have used may not be adapted any longer. Indeed, despite the use of a rigorous model for the incident optical field computation, the diffraction and resonance effects at the sphere are neglected. As argued by Ashkin [10] following comparisons by Hulst [28] between scattering predicted by the ray-optics and the exact angular distribution of the Mie theory, the ray-optics approach can give reasonable predictions for sphere size parameters $2\pi a/\lambda$ greater than 10 to 20. This cor-

#10213 - $15.00 USD Received 4 January 2006; revised 3 February 2005; accepted 10 February 2006

responds to a sphere diameter of more than 3 to 6 μm for a $1\mu m$ laser in water. Thus the model is used at the limit sphere-sizes for its validity, which may explain why measurements on $7\mu m$ beads are better reproduced by this theoretical model. Particle sizes of 5 and $7\mu m$ were chosen because using larger particles the inertial terms in the motion equations (10) may become significant. For smaller beads, on the other hand, the axial-position measurement technique we used was not applicable anymore, in addition to the fact that the ray-optics model for the force calculation may not be justified any longer.

For both sphere-sizes, the measured axial equilibrium position z_0^{eq} at increasing transverse positions r_0 is not monotonically increasing but rather shows oscillations. This effect may in part be attributed to the spherical aberrations created by the coverglass-water interface, as predicted by the VD model (Fig. 6(c)), and we observed that this effect was more pronounced at larger trapping depths. However, these oscillations are also very likely to be a signature of geometrical resonance [12, 16, 18] not considered by the present model.

An interesting point concerns the effects of the spherical aberration (SA) induced by the refractive index mismatch at the coverslip-water interface. SA are well known to be responsible for a reduced axial trapping efficiency due to the degradation of the axial intensity gradients. Nevertheless, the lateral degradation of the intensity gradients is less important, which could suggest that lateral trapping forces are also less concerned. Our results, showing the interplay between axial and transverse forces, clarify the reasons for the strong reduction in the maximal transverse trapping efficiency due to SA. The correction of the SA may allow for stronger maximal transverse forces when trapping deeper into the specimen chamber [29, 30, 31] mainly because the escape would take place at larger transverse positions. On the other side, it is very likely that the SA has less effect on the trap stiffness (restoring forces close to the optical axis), as predicted by the theoretical model (see Fig. 6(d)). Thus equipartition-based force calibrations would be less concerned by SA.

Finally, these results may suggest that optical tweezers based on Laguerre-Gaussian beams, which were proven to provide an increased axial trapping efficiency for larger particle sizes [20, 21], may also allow for an increased transverse trapping efficiency [17]. However, the deduction is not straightforward since an increased axial trapping efficiency *on-axis* does not imply that the axial trapping efficiency *off-axis* is increased, or that the transverse position area presenting an axial equilibrium position is extended. Nevertheless, any precise mathematical comparison between the maximal transverse forces obtained with focused Gaussian beams and those obtained with other types of beams has to take these axial equilibrium conditions into account.

6. Conclusion

The presented results clarify the interplay between the transverse and axial trapping forces. We have demonstrated that the axial equilibrium position of a dielectric microsphere trapped by optical tweezers and submitted to a purely transverse external force (e.g. fluid flow) depends on the microsphere transverse position in the trapping beam. In particular, our results show that the beads escape the trap at transverse positions close to $r_0/a \simeq 0.6$, indicating that the escape is due to a failure in the axial trapping at that distance from the optical axis, and not because the maximal transverse force is reached. We have proven by comparing a mathematical model to experimental measurements that any reliable mathematical prediction of the maximal transverse forces has to take these essential axial equilibrium issues into account.

#10213 - $15.00 USD Received 4 January 2006; revised 3 February 2005; accepted 10 February 2006